

Trabajo Fin de Máster
Máster en Nuevos materiales

**Magnetic nanoparticles and composites for
applications: focus on electrophysical
techniques.**

Nanopartículas y composites magnéticos
para aplicaciones: enfoque en las técnicas
electrofísicas.

Autor/a:

Laro Media Ranero

Realizado en:

Facultad de ciencias y tecnología UPV/EHU

Director/a:

Galina V. Kourliandskaia

Leioa-Santander, junio de 2022.

Abstract.

Nanoparticles are becoming very important in the last decades providing great advances in different scientific fields such as biomedicine, the miniaturization of electronic devices or the manufacture of nano sensors. That is why, throughout this work we will characterize the properties of a series of nanoparticles of aluminium, iron and iron oxide, in order to know their characteristics and their possible applications. The curious thing about the particles with which we are working is that they have been synthesized through novel methods that have not yet been established at the industrial level, the electrophysical methods. These methods are the electric wire explosion method, which consists of generating particles by causing a discharge in a conductive wire, and the laser evaporation method.

Magnetic properties, microwave absorption properties and structural and compositional characteristics of nanoparticles or composites with particles are studied. From the results obtained we will see which are the applications for which the different types of particles are useful depending on their behavior under these external stimuli.

Resumen.

Las nanopartículas están tomando mucha importancia en las últimas décadas aportando grandes avances en diferentes ámbitos científicos como la biomedicina, la miniaturización de dispositivos electrónicos o la fabricación de nanosensores. Es por ello, que a lo largo de este trabajo se caracterizarán las propiedades de una serie de nanopartículas de aluminio, hierro y óxido de hierro, con el fin de conocer las características de las mismas y sus posibles aplicaciones. Lo curioso de las partículas con las que se trabaja es que se han sintetizado a través de unos métodos novedosos que aún no se han instaurado a nivel industrial, los métodos electrofísicos. Estos son el método de explosión de cable eléctrico, que consiste en generar partículas provocando una descarga en un cable conductor y el método de evaporación por láser.

Se estudian las propiedades magnéticas, las propiedades de absorción de microondas y las características estructurales y de composición de las nanopartículas o composites con partículas. A partir de los resultados obtenidos veremos cuales son las aplicaciones para las que son útiles los diferentes tipos de partículas en función de su comportamiento bajo estos estímulos externos.

Acknowledgements.

First of all, I want to thank Galina, the director of this work, for being able to work with her, for her help and dedication. It has allowed me to continue advancing in my knowledge about nanoparticles and composites and how to work in the different laboratories when taking measurements.

I thank the staff of the electron microscopy research services of the University of the Basque Country, especially Dr. Saioa Suarez, who took care of the SEM measurements and with whom I learned how to handle the instrument.

I would also like to thank Dr. Aitor Larrañaga, who taught me important aspects of crystallography and with whom the X-ray diffraction and X-ray fluorescence measurements were taken.

I thank Dr. Iñaki Orue for teaching me different methods of sample preparation for VSM magnetic measurements.

Finally, I thank Dr. Luis Lezama for teaching me how to prepare the samples and take FMR measurements.

Index.

1.Introduction.....	5
2.Objectives.....	6
3. Synthesis and characterization technique.....	6
3.1. Synthesis techniques.....	7
3.1.1. Electrical explosion of wire.....	7
3.1.2. Laser target evaporation.....	8
3.1.3. Synthesis of composites.....	8
3.2. Characterization techniques.....	9
4.Materials.....	12
4.1. Nanoparticles.....	12
4.2. Composites' matrix.....	12
5. Results.....	13
5.1. Structural and compositional characterization.....	13
5.1.1. X-Ray characterization.....	13
5.1.2. Microscope characterization.....	18
5.2. Magnetic characterization.....	22
5.2.1. Analysis of powder samples.....	22
5.2.2. Analysis of ES-X% composites.....	23
5.2.3. Analysis of composites with 2 and 4 drops of lacquer.....	24
5.3. Microwave absorption.....	25
5.3.1. Transmitter-receiver.....	25
5.3.2. Ferromagnetic resonance.....	27
6.Conclusions.....	29
7.References.....	30

1. Introduction.

Nanoscience research is opening up a wide range of applications in which nanoparticles play an important role. Magnetic nanoparticles (MNPs) of iron oxides have long been of special interest due to their properties, which are suitable for a wide range of biomedical, environmental and technological applications.

The different properties of both individual nanoparticles and resin-synthesised composites are studied. The behaviour of the samples is tested in different tests to check how their magnetic and microwave radiation absorption properties vary. In addition, their structural and compositional properties are also studied in order to check how the size of the nanoparticles or their distribution in the composite influences the behaviour of the samples in response to external stimuli.

In this work we work with four different types of particles, these are: aluminium particles, which will be referred to throughout the article as Al, iron particles obtained through laser targeted evaporation, which will be shown as LTE, iron particles, named as Fe and commercial magnetite particles, called AA, which are used as a reference to compare the results of the particles obtained by electrophysical methods with those of particles already used in the industry.

In addition, resins are used for the synthesis of certain composites that will be used as samples in different tests. Synthesis of composites with resin or lacquer provides good adhesion to metals, improved mechanical properties, chemical stability, as well as retaining the electromagnetic properties of their fillers. Samples will be synthesised with a commercial epoxy resin containing m-phenylenediamine, with a ratio of the curing agent determined to be 22%. The resin used for these composites is KDA-2, synthesised at Khimeks Ltd., Russia [1]. As for the lacquer used for the analysis of other types of samples, we have a resin, polyvinyl butyral (PVB), a random terpolymer composed mainly of vinyl alcohol and vinyl butyral with relatively small amounts of vinyl acetate. A terpolymer is a copolymer in which two or more chemically distinct monomeric units alternate along irregularly shaped linear chains. PVB is a colourless, amorphous thermoplastic resin, which is widely used in technological applications such as laminated automotive glass, paints and adhesives, due to its excellent flexibility, its ability to form film-like coatings, its good adhesion properties and its excellent UV resistance [2][3].

The electrophysical techniques of nanoparticle synthesis allow, by varying the manufacturing conditions, to obtain particles with sizes and shapes suitable for the different applications for which they will be used. This enables significant advances in advanced materials science, such as nanodevices, miniaturisation of electronic devices or their use in biomedical applications [4]. Nanoparticles are attractive in this regard because of their peculiar optical, electronic, magnetic and catalytic properties, many of which can be modulated simply by changing their size, shape, or the functionalisation of the nanoparticle surface, without changing the composition of the material. Nanoparticle synthesis methods fall into two categories, the first (top-down) consisting of the splitting of bulk solids into smaller portions. This approach can involve grinding or attrition, chemical methods, and volatilisation of a solid followed by condensation. The second (bottom-up) approach involves the fabrication of nanoparticles through the condensation of atoms or molecular entities in a gas phase or in solution. Another fundamental aspect of nanoparticle synthesis is their stabilisation, so that their size and shape can be maintained over time without losing the properties they possess after synthesis.

Until now, nanoparticle synthesis methods have relied on wet chemistry methods to synthesise high-quality nanoparticles from a variety of inorganic materials such as gold, silver, iron oxide and semiconductors [5][6]. Despite the good properties of the particles synthesised by these methods, new fabrication methods have emerged, the electrophysical methods, which are the subject of this work.

These methods are the electric explosion wire method (EEW) and the laser target evaporation method (LTE). These two methods, based on electrophysical interactions with a source material, allow the synthesis of nanoparticles with high interest for materials science due to the properties they possess. The EEW method is based on the contact of a wire between two electrodes under a potential difference, which causes an explosion, in which the wire evaporates forming particles of different sizes that are subsequently filtered. It can be used to produce nanoparticles cheaply and efficiently at a rate of 50-300 grams per hour and with a purity of over 99%, the process requires relatively low energy consumption, effects on the environment are minimal because the process takes place in a closed system and particles can be as small as 10 nm, but are typically less than 100 nm in diameter [7]. The LTE method is based on the interaction between a laser and a source material, which due to the incidence of the laser starts to evaporate forming nanoparticles. From this process it is intended to obtain nanoparticles of diameters around 10 nm, spherical and disaggregated with a narrow size distribution and an improved effective magnetization. Between 100 and 200 g of particles are generated in one batch [8].

The properties of the particles synthesized from these two methods will be comparatively analysed in different characterization tests, x-ray diffraction, optical microscopy and SEM microscopy, magnetization and microwave absorption.

2. Objectives.

The main objective of the work is the characterization of the different types of nanoparticles obtained from these two methods. Study their magnetic, structural and microwave radiation absorption properties and see how they change depending on the type of particle, its size or the concentration in which they are found in a composite. In this way, it will be possible to verify the possibility of using these nanoparticles in different applications based on their characteristics, such as magnetic sensors, hyperthermia systems in biomedical applications or devices immune to microwave radiation.

Although the one mentioned above is the main objective, there are a series of objectives, which, although they are secondary, are just as important. These allow me as a student to know the different techniques applied to nanoparticles and the work methods in the laboratories of the faculty. Among these objectives are the learning of the use of optical microscopes and SEM, and the subsequent analysis of the images obtained, which allow knowing the size of the particles and their distribution in the composites. The learning of X-ray diffraction and X-ray fluorescence techniques and the use of their test instruments, which allow knowing the structural properties of the samples and their compositional characteristics. The magnetic and microwave absorption analyses allow knowing the operation of the VSM devices and microwave radiation emitter and the subsequent interpretation of the data obtained. In addition, the learning of composite synthesis for its subsequent analysis or of the matrices that are used for microwave absorption measurements.

All the synthesis of composites and measurements carried out throughout the investigation have been carried out by me, or failing that in my presence, therefore I know how the devices work and how to use them. That is why the development of this work has been a very enriching experience for me as a student in my training process as a researcher.

3. Synthesis and characterization techniques.

In this section we will learn about the different methods of synthesising nanoparticles by means of electrophysical methods. Each is capable of producing particles that differ in size, shape or even the total amount that each is capable of synthesising in a single process.

We will also learn about the different techniques used for the characterization of particles and composites. Magnetic properties, microwave radiation absorption properties and structural properties will be characterized.

3.1. Synthesis techniques.

3.1.1. Electrical explosion of wire:

EEW is a process of rapid transition of metal wire from a conductive state in a non-conductive by passing through the wire a high-density current pulse. In this case the transition of the conductor material from the solid state into a dense plasma occurs to form a fine metal particle which are the nanoparticles. The resistive heating vaporizes the wire, and an electric arc through that vapor creates an explosive shockwave. The particle size depends on the energy and temporal characteristics of the current pulse flowing through the conductor. Recently the effect of EEW is used for obtaining of metal nanoparticles in different application.

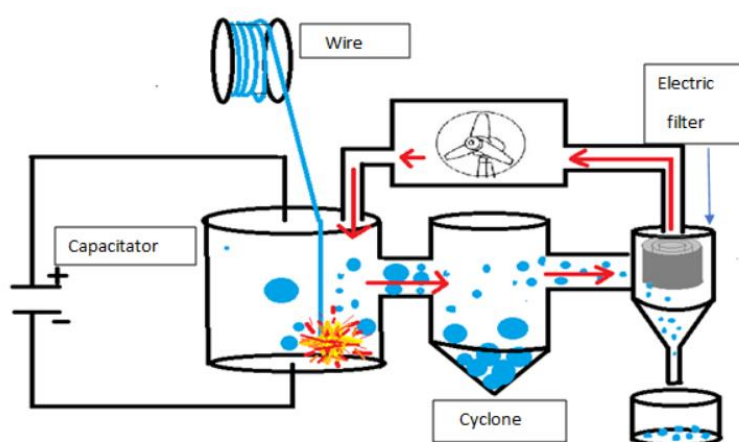


Figure 1. Schematical representation of electrical exploding wire technique.

The basic components required for the exploding wire method are a thin conductive wire and a capacitor. The wire, which is the source of nanoparticles, is usually made of gold, aluminium, iron or platinum, and is typically less than 0.5 mm in diameter. A current density discharge of $10^4 - 10^6$ A/mm² is generated, causing temperatures of up to 100,000 K.

The process is as follows, an upward current, supplied by the capacitor, flows through the wire. The current heats the wire by ohmic heating until the metal begins to melt. The metal melts forming a broken series of imperfect spheres that vaporize. The metal vapor creates a path of least resistance, allowing even greater current to flow. An electric arc is formed that converts the vapor into plasma, which expands, creating a shock wave. Electromagnetic radiation is released along with the shock wave.

Nanoparticles are created when the ambient gas in the system cools the vaporized metal. EWM can be used to produce nanoparticles cheaply and efficiently at a rate of 50 to 300 grams per hour [9] and with purity greater than 99%. The process requires relatively low energy consumption, as little energy is lost in the conversion from electrical to thermal energy. Particle sizes are between 10 and 100 nm. The properties of the powder can be altered depending on the parameters of the explosion.

When EEW is performed in a standard oxygen-containing atmosphere, metal oxides are formed. Pure metal nanoparticles can also be produced with EEW in an inert environment, typically argon gas or distilled water. Pure metal nano powders must be kept in their inert environment because they ignite when exposed to oxygen in the air, which is why passivation of the particles is necessary to avoid risks [10].

The demand for metal nanoparticles, and therefore production methods, has increased as interest in nanotechnology has grown. Despite its overwhelming simplicity and efficiency, it is difficult to modify the experimental apparatus for use on an industrial scale. Therefore, this technique has not yet been widely used in the materials production industry due to manufacturing quantity problems.

3.1.2. Laser target evaporation:

The method can be considered as an evolution of the laser vapor deposition technique. In the case of laser deposition, the material is evaporated by a laser beam and then deposited on a suitable substrate.

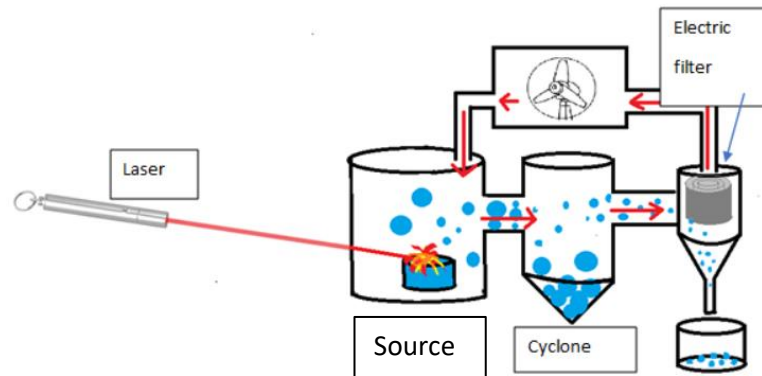


Figure 2. Schematical representation of laser target evaporation technique.

In the case of LTE the material vapours are cooled in the gas phase resulting in condensation of the nanoparticles. The spherical shape of the particles is due to the fact that evaporation takes place in a circulating gas flow, which cools the vapor and prevents the particles from agglomerating. A laser, usually of ytterbium fiber with a wavelength of 1.07 μm , was used for the preparation of the LTE MNPs [11].

The pellet, from which the nanoparticles (of Fe_2O_3 , for example), 65 mm in diameter and 20 mm in height, were formed, was pressed from micron-sized coarse powder. In the evaporation chamber, the target pellet was mounted on a drive mechanism, which allows both its rotation and longitudinal movement. The laser beam was focused on the pellet surface. The focal spot diameter was 0.45 mm. The drive mechanism provided a beam sweep speed of 20 cm/s on the target surface, which ensured uniform wear of the target surface. The laser was operated in a pulsed regime, which favoured the formation of fine, uniform MNPs with a narrow particle size distribution. The oxide vapours drifted away from the focal spot and condensed into spherical MNPs, which were entrained by the working gas to the cyclone and fine filter where the dust was collected.

The only particles used in this research synthesized from this technique are known as LTE, Fe-core nanoparticles with a very thin outer layer of iron oxide for passivation.

3.1.3. Synthesis of composites.

Two different types of composites are developed which are composed of spherical nanoparticles together with an epoxy resin matrix or a lacquer matrix.

For the synthesis of epoxy resin composites, the two components of the resin are mixed in appropriate quantities and mixed by means of a glass rod, once the resin is homogeneous, the different concentrations of microparticles are added to be distributed without forming agglomerates also stirred with a glass rod, thus forming the composites called ES-X%.

Sample name:	MNP's concentration
ES-0	0.0%

ES-1	1.0%
ES-2	2.0%
ES-5	5.0%
ES-9	9.2%
ES-20	20.0%
ES-30	30.1%
ES-50	50.1%
ES-70	70.1%

Table 1. Table of composites synthesised with epoxy resin.

As shown in the table above, 9 samples with different concentrations were synthesised. However, in this work, only the properties of ES-0, ES-1, ES-2, ES-5, ES-9 and ES-30 composites are analysed.

The lacquer composites are synthesized inside capsules, in which initially the exact quantity of particles is introduced, then with a pasteur pipette the appropriate drops are added to match the desired concentration and so that the result of the composite is homogeneous and reducing the amount of agglomerates, the capsule is shaken with care not to spill the mixture.

Composites' name	N° of samples	N° of laquer's drops	MNP's [mg]
Al-C	20	2	8.31 mg
Fe-C	20	2	8.25 mg
LTE-C	20	2	8.20 mg
AA-C	20	2	8.20 mg

Table 2. Table of composites synthesised with lacquer.

3.2. Characterization techniques.

For compositional characterization, the Ametec "Spectromidex" XRF device and a Philips X'Pert, PRO x-ray diffraction device is used. X-ray fluorescence is an analytical technique for determining the chemical composition of a wide variety of sample types. In our case, the samples, particles of different materials or synthesised by different methods to be analysed, are in powder form. However, the technique also allows the determination of the thickness or composition of different layers. XRF is an atomic emission method that allows the wavelength and intensity of the "light" (X-rays in this case) emitted by energised atoms in the sample to be measured. In XRF, irradiation by a primary X-ray beam from an X-ray tube causes the emission of fluorescent X-rays with discrete energies characteristic of the elements present in the sample. In this way, the fluorescent radiation emitted by the sample reaching the detector can provide not only qualitative but also quantitative information about the sample. In other words, it is known which elements make up the sample and also their concentration [12]. An X-ray beam is incident on the sample. The beam scattering originates from an aggregate of atoms, in a crystal, where the phase relationships are fixed and repetitive, the scattering profile becomes defined peaks. In this case, the total effect is known as diffraction. Diffraction can therefore be defined as co-operative reflection from different parallel planes, defined by lattice atoms. The light incident on the sample will only diffract when the ratio between the incident angle and the emergent angle follows Bragg's Law:

$$2d \sin \theta = n\lambda \quad (1)$$

The diffractometer is equipped with a generator that supplies power to an X-ray tube, a precision goniometer that allows synchronised rotation at θ and 2θ , i.e. if the sample travels through an angle θ , the goniometer travels through an angle 2θ at the same time, a sample holder that rotates in solidarity with the axis of the goniometer, a detector in charge of capturing the diffracted X-radiation and an electronic control unit, which allows the edition of a series of parameters for data acquisition [13][14].

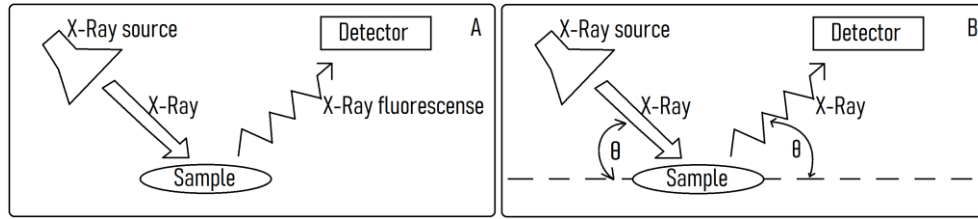


Figure 3. Schematic representation of A) XRF and B) x-ray diffraction.

For the structural analysis of the samples an optical microscope is used, which allows to take images with different magnifications of the samples up to a maximum resolution of about 200 nm due to the incident wavelength [15]. For this reason, a SEM (scanning electron microscope), in the faculty the JEOL JSM-7000F, is used to complement the optical microscope, which is an electron microscope that allows taking high-resolution images of the surface, 10 nm of resolution. This is due to the use of an electron beam as a source of illumination, which is obtained by the excitation of a metal filament (cathode) and is attracted by the potential difference produced by the anode, provided they are in a vacuum. Its operation is based on the interactions of the electrons coming from the microscope with the sample. The difference with a conventional microscope is that it emits a beam of electrons instead of a beam of light. In the scanning electron microscope, it is necessary to accelerate the electrons in an electric field by means of a potential difference. For very sensitive samples, such as biological samples, small voltages are used, and for metallic samples high voltages are used, as they are more resistant and allow shorter wavelengths to be used, which increases the resolution of the images taken by the microscope. The accelerated electrons coming out of the gun are focused with lenses, so that as few electrons as possible are incident on the sample to obtain better resolution. Deflector coils sweep this fine beam of electrons over the sample, spot by spot. This is another method used to characterize samples and check that their composition is correct. In other words, by means of these images taken we can check that the samples contain the correct percentages of particles [16].

In order to know the magnetic properties of the particles and composites, a VSM device, vibrating sample magnetometer, is used to measure the magnetic moment and magnetization of the samples from the Faraday induction law. The sample, vibrating at a given frequency, is subjected to a magnetic field varying between -2 and 2 T. The magnetic field must be strong enough to completely saturate the samples and uniform throughout the sample space. The external field is applied parallel to the length of the sample and the hysteresis loop is obtained. A vibrating sample magnetometer measures the magnetic moment of a sample when it vibrates in the presence of a static magnetic field, from which magnetization and magnetic susceptibility can be determined. It stands out for its versatility, simplicity, allowing accurate and reliable results to be obtained, and it is also inexpensive [17][18].

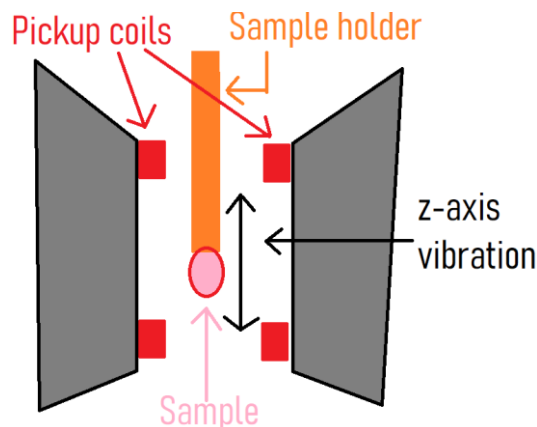


Figure 4. Schematic VSM instrument.

To characterize the microwave absorption properties, two tests are performed, one by means of a faculty emitter-receiver device and an FMR measurement of the samples, with the Bruker ELEXSYS device. A transmitter-receiver system will be used, in which the transmitter uses a wave with a wavelength of 2.85 cm and a receiver which can amplify the received signals. The transmitter, a gun diode, emits a coherent, linearly polarised wave. The gun diode acts as a non-linear resistor that oscillates in the microwave band, radiating a microwave beam along the bell axis. The receiver, which reads low amplitude signals, is proportional to the received microwave signal strength. This receiver consists of a Schottky diode in a resonant cavity, only responding to the wave that is polarised along the axis of the diode [19][20].

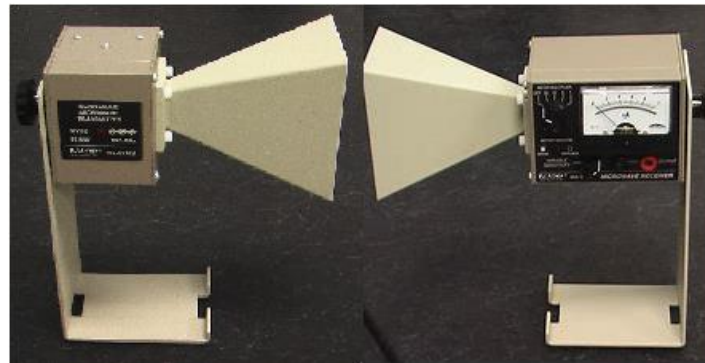


Figure 5. Microwave transmitter and receiver.

Ferromagnetic resonance describes the resonant absorption of electromagnetic radiation, usually microwave, in a magnetic material containing strongly exchange coupled electrons. Absorption is measured as a function of the applied magnetic field, in our case, absorption's derivative as a function of the magnetic field applied. It encompasses any system containing a high concentration of paramagnetic ions with predominantly ferromagnetic exchange coupling. Ferromagnetic resonance, or FMR, is the coupling between an electromagnetic wave and the magnetisation of a medium through which it passes. This coupling induces a significant power loss of the wave. The power is absorbed by the precessing magnetisation (Larmor precession) of the material and is lost as heat. This effect can be used for various applications, such as spectroscopic techniques or the design of microwave devices. The device works to take measurements at a frequency of 8.85 GHz [21][22].

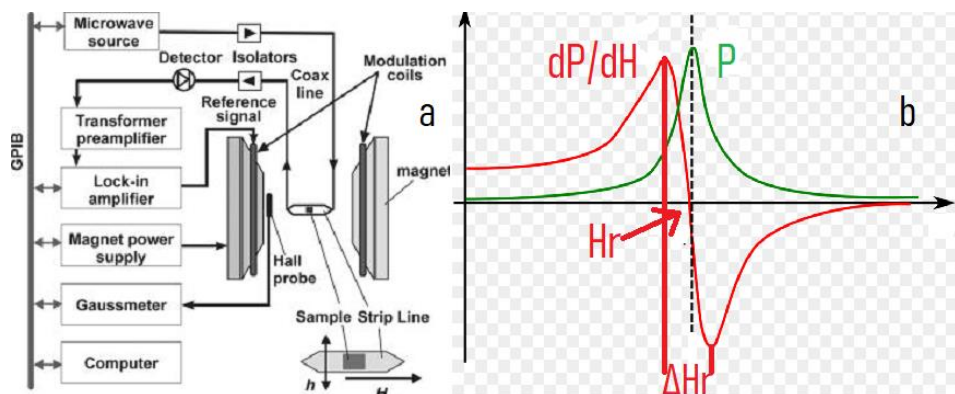


Figure 6. a) Schematic of FMR. b) Typical FMR plots.

In figure 6.b we can see the type of curve that is obtained if the absorption is resonant and the derivative of the absorption versus magnetic field is shown in red and the absorption as a function of H in green. In addition, we can see marked certain points of interest in the red curve, such as the resonance field (H_r) or the field variation between peaks (ΔH_r), which are important parameters of the ferromagnetic resonance of each material.

4. Materials.

In this section we will present all the materials used throughout the research, not only the nanoparticles, also the different resins or lacquers used for the synthesis of different composites.

4.1. *Nanoparticles.*

Four different types of aluminium and iron nanoparticles have been used for the development of this project. There is only one type of aluminium nanoparticles, manufactured by the electric wire explosion method, a very favourable method for this material, since it has good conductivity. These particles will be referred as "*Al*" throughout this work.

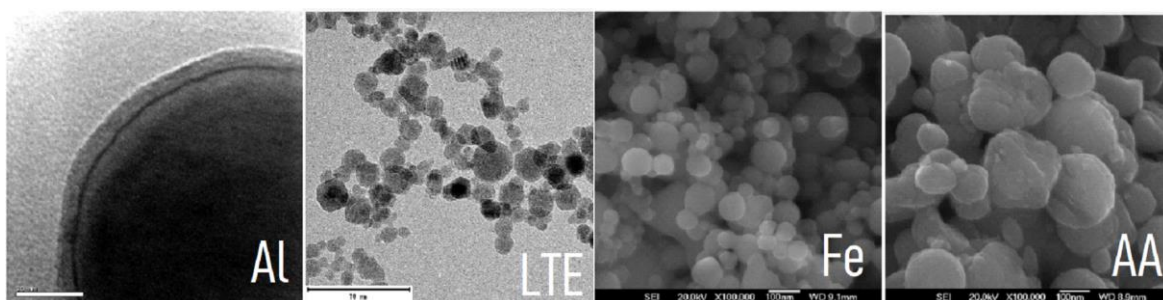


Figure 7. SEM and TEM images of the nanoparticles.

As can be seen in figure 7, a SEM image, the particles have a high purity aluminium core, with a diameter of between 80 and 100 nm and a layer of about 5 nm of aluminium oxide that serves to passivate the nanoparticles.

Regarding the iron particles, 3 different types are used, some manufactured by the laser target evaporation method, others manufactured by the electric wire explosion method and the last ones are commercial Alpha Hesar magnetite particles, which serve as a reference to compare how the properties of the rest of the particles vary and check their efficiency in different applications.

The image on the upper right is a TEM image of the Fe nanoparticles fabricated by the LTE method, which will be referred to as "*LTE*" throughout this work. As can be seen, they are nanoparticles of between 10 and 20 nm whose geometry is not very spherical.

The down left image shows an image taken by a SEM microscope of the Fe particles synthesized by means of the EEW technique. These particles will be referred to as "*Fe*" throughout this work. As can be seen in the image, they are particles of about 100 nm in diameter and with an exceptional spherical shape. They have a high purity iron core surrounded by a thin layer of iron oxide that favors their passivation.

Finally, we have the commercial magnetite particles, which will be referred to as "*magnetite*" or "*AA*" throughout this work. As can be seen in figure x, the particles have diameters well over 100 nm, a shape that is far from spherical and a wide size distribution.

4.2. *Composites' matrix.*

For the development of this research, two types of composites have been used, formed by a matrix to which different concentrations of the different particles mentioned above are added. The study of the properties acquired by these composites when nanoparticles are added is of great importance, since their electromagnetic or radiation absorption properties are combined with the mechanical properties of the

composite matrix. It is also thanks to these matrices that the composites acquire shape, consistency and become easier to handle and work with.

For this reason, in order to study how the properties of the nanoparticles change, an epoxy resin and a lacquer are used as matrices in this research.

The epoxy resin KDA-2 is used for the synthesis of composites whose fillers are magnetite nanoparticles, which will be called ES-X%, where X is the percentage concentration of iron powders in the composite. This resin is a combination of ED-20, formed by the condensation of 4,4'-isopropylidenediphenol and epichlorohydrin, mixed with DEG-1, formed by diethylene glycol diglycidyl using m-phenylenediamine as a curing agent. This allows the resin to acquire interesting properties, such as an individual stoichiometric compound of definite structure and the curing temperature is high. It has been shown that the addition of nanoparticles synthesised by EEW does not affect the thermodynamics of the cure regardless of their concentration [1].

As for the resist used for the analysis of other types of samples, we have one resin, polyvinyl butyral (PVB), a random terpolymer composed mainly of vinyl alcohol and vinyl butyral with relatively small amounts of vinyl acetate. A terpolymer is a copolymer in which two or more chemically distinct monomeric units alternate along irregularly shaped linear chains. PVB is a colourless, amorphous thermoplastic resin, which is widely used in technological applications such as laminated automotive glass, paints and adhesives, due to its excellent flexibility, its ability to form film-like coatings, its good adhesion properties and its excellent UV resistance [2].

These composites are synthesised inside a capsule, with the aim of being studied by means of two tests. The first, in which an individual capsule is analysed for its magnetic properties in VSM. The second, for microwave absorption analysis, for which 20 identical capsules are glued onto a plastic sheet.

5. Results:

Different techniques for the characterisation of nano and microparticles are carried out in order to know their properties, their composition, their structure and also their magnetic response.

The different results obtained from the samples analysed by means of the following techniques will be shown below.

5.1. Structural characterisation.

5.1.1. X-Ray characterization.

X-ray fluorescence.

The following X-ray fluorescence results were obtained for the different particle samples:

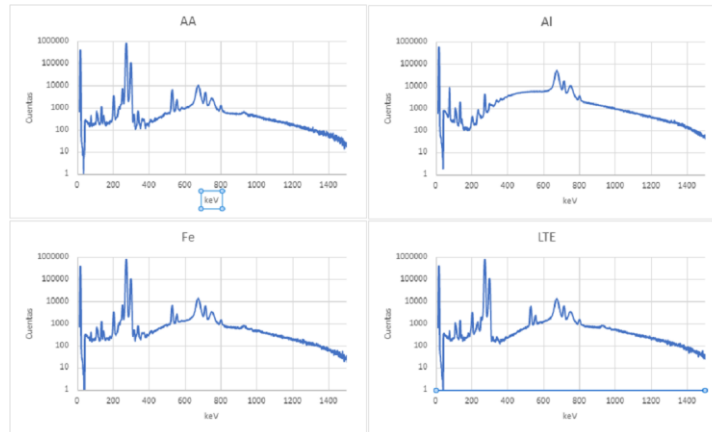


Figure 8. X-ray fluorescence diagram of the different particles.

The software integrated in the fluorescence instrument is able to identify peaks, which correspond to characteristic signals of certain elements. In this way it is obtained:

	Components [%]		
AA	91.45% Fe	2.34% S	1.33% Al
Al	98.38% Al	<0.10% Fe	
Fe	91.61% Fe	<0.73% Al	
LTE	92.34% Fe	1.12% S	

Table 3. Component's concentration of each sample XRF.

The AA sample corresponds to Alpha Hesar magnetite, so the fluorescence results obtained fit with the expected high percentage of iron and very low concentrations of sulphur and aluminium, which may be due to additional impurities from the synthesis or processing of the particles.

For the aluminium sample, expected results are obtained, corresponding to aluminium particles of very high purity, taking into account that certain components appear which are due to the contributions of the X-ray tube.

The Fe sample also gives the expected results, with a high concentration of iron and very low concentrations of impurities.

For Fe particles synthesised by the laser targeted evaporation process (LTE), a high concentration of iron is obtained together with low concentrations of impurities, such as sulphur. This Fe sample can be considered to be of high purity.

As can be seen in all the figures for each of the samples, a series of peaks appear between 600 and 800 keV, these peaks are characteristic of elements such as Indium, Cadmium or Silver, among others, which correspond to the X-ray emissivity tube. This is why, although these elements appear in certain percentages of the composition of the samples when taking the measurements, we know that their appearance is due to their emission from the X-ray fluorescence equipment [12].

X-ray diffraction

X-ray diffraction (XRD) is one of the most effective techniques for the qualitative and quantitative analysis of crystalline phases of any type of material. In order to be able to submit the sample to this analysis, prior preparation of the sample is required. Although it allows the analysis of solid pieces, the sample was analysed in the form of a fine, homogeneous powder. This powder was placed in the sample holder of the laboratory's X-ray diffractor, which was previously cleaned with alcohol to avoid contamination of the sample.

The data obtained are plotted on a graph as the intensity of the diffracted light as a function of the angle 2θ . Where the position of the intensity maxima depends only on the cell parameters, so that both cell parameters and Miller indices can be obtained. And where the intensity of the maxima only depends on the structural model of the sample.

From the data obtained we can know the different phases that compose the samples, their cell parameters, and by analysing the characteristic peaks we can know the crystal size from the Scherrer's formula:

$$\tau = \frac{K\lambda}{\beta \cos \theta} \quad (2)$$

Where τ is the mean size of the ordered (crystalline) domains, K is a dimensionless shape factor, λ is the X-ray wavelength, β is the line broadening at half the maximum intensity (FWHM) and θ is the Bragg angle [23].

For the different particles, the following diffraction spectra were obtained:

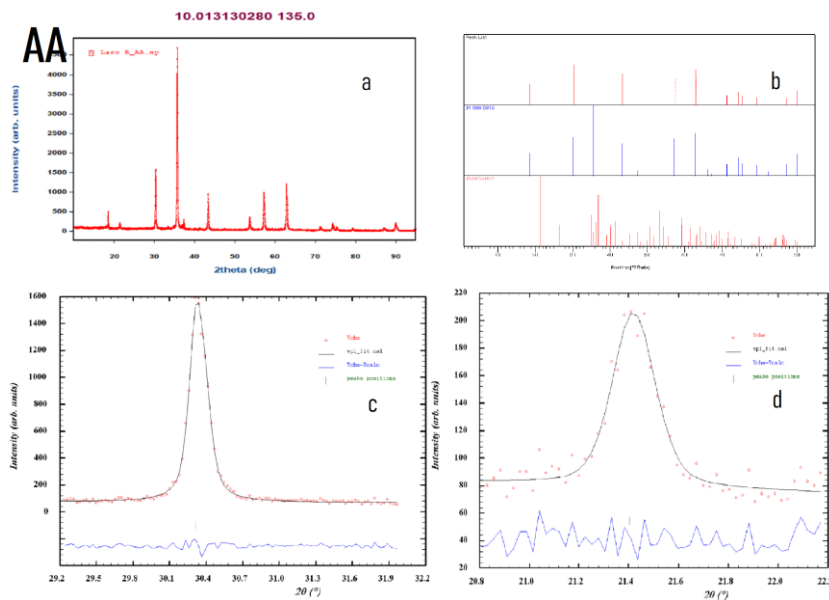


Figure 9. a) X-ray diffractogram of AA powder; b) Different phases that make up X-ray diffractogram of AA powder; c) Characteristic peak of magnetite phase; d) Characteristic peak of goethite phase.

By means of the diffractometer software, used in the laboratory, we can obtain the following information from the diffraction data obtained. By analysing the 2θ positions of the maxima in the intensity we can not only know the composition of the samples, but also obtain information about their structure and the parameters of the unit cell.

As can be seen in figure 9, the diffractogram has high intensity and narrow peaks, which corresponds to high crystallinity.

For the sample AA, the intensity peaks in the diffraction diagram, through the software that compares it with a wide range of different diffractograms, correspond to the following substances:

In the upper right figure, we can see 3 graphs, the first one corresponds to the intensity peaks obtained experimentally, the second graph, in blue, corresponds to the contribution to the diffractogram of magnetite Fe_3O_4 and the lower red graph corresponds to the contribution to the diffractogram of goethite $\text{FeO}(\text{OH})$. From the relations between the intensities obtained experimentally and the substance register, we can obtain approximately the proportions of each substance in our sample, in this case, 92% Fe_3O_4 and 8% $\text{FeO}(\text{OH})$. The possible cause of the appearance of the goethite phase may be that, in

contact with the atmosphere, the Fe₃O₄ magnetite nanoparticles have absorbed hydrogen and oxygen to form this new, sparse structure in the sample.

From the graph b) it is obtained that the composition of the sample consists of 2 phases, magnetite and goethite. By analysing the width at mid-height of the characteristic peaks of each structure, figure c) and d), we can calculate the size of the crystals that compose it. In this way, for magnetite, from the angle 2 Theta and the width at half height, by means of the scherrer relation we obtain that the size of the crystals of Fe₃O₄ are **~240 nm**. For goethite, through the same relation we obtain that the size of its crystals is **~90 nm**.

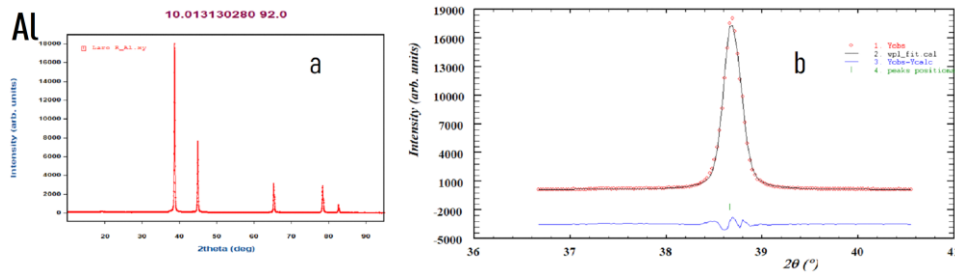


Figure 10. a) X-ray diffractogram of Al powder. b) Characteristic peak of aluminium phase.

The figure above shows the diffractogram of the aluminium powder sample. As can be seen in figure a), the diffractogram has high intensity and narrow peaks, which corresponds to high crystallinity. In the following, it will be shown that the composition is as expected and we will see what structure the particles that make up the sample have.

From the diffractogram we can see that the composition of the sample is pure aluminium, since the experimental diffractogram has the same 2 Theta angles as the register of the aluminium. It should be clarified that certain intensity maxima appear as dotted lines, which are due to the interactions $k\alpha_1$ and $k\alpha_2$.

As with the previous sample, a peak of intensity characteristic of the phase can be taken, with its 2Theta angle and its width at half height, the approximate size of the crystals can be calculated applying Scherrer's formula, an approximate crystal size of **~115 nm** is obtained.

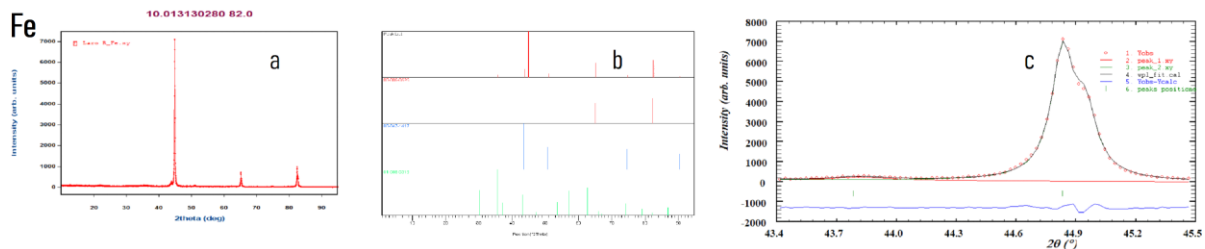


Figure 11. a) X-ray diffractogram of Fe powder. b) Different phases that make up X-ray diffractogram of Fe powder. c) Characteristic double peak belonging to the two phases.

The figure above shows the diffractogram of the iron particles obtained through the wire explosion process. As can be seen in figure a), the diffractogram has high intensity and narrow peaks, which corresponds to high crystallinity. From this figure, compositional and structural information of the sample is obtained.

The figure above shows the different phases that make up the sample, with a main phase of ferrite with two other phases, taenite and magnetite, in smaller proportions. The figure shows 4 diffractograms, corresponding from top to bottom to the experimental diffractogram, the ferrite diffractogram, the taenite diffractogram and the magnetite diffractogram respectively.

From the graph b) it is obtained that the composition of the sample consists of 3 phases, ferrite, taenite and magnetite. To simplify the process, for the Fe sample, two joint characteristic peaks are analysed, the lower one corresponding to the taenite phase and the higher one to the ferrite phase. In this way, with the data obtained and applying the scherrer formula, we obtain taenite crystal sizes of **45 nm** and ferrite of **240 nm**. In addition, another phase appears in this sample, magnetite, to know its crystalline dimensions we proceed to analyse a characteristic peak of magnetite, but its contribution to the diffractogram is so small that we cannot obtain data on its crystalline dimensions.

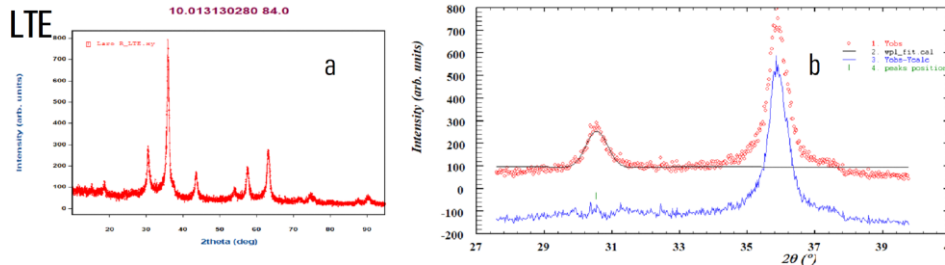


Figure 12. a) X-ray diffractogram of LTE powder. b) Characteristic peak of magnetite phase.

The diffractogram of the particles obtained from the LTE process is analysed in order to know their structure and composition. As can be seen in the figure above, the diffractogram of these particles is different from the previous ones, with wider peaks and a larger background, which may correspond to a lower crystalline order, more amorphous with smaller crystal sizes.

As can be seen in the image above, the experimental diffractogram matches that of the magnetite software log. Therefore, we have a similar structure to that of sample AA, but in this case we assume a smaller crystal size. From the diffractogram obtained we can calculate the crystal sizes of each phase by analysing the characteristic intensity peaks of each phase. In this case the same characteristic peak of magnetite was analysed as for sample AA. In this way, by means of the Scherrer ratio, the position of the 2Theta angle and the width of the peak at half height, we obtain the following sizes for the magnetite crystals **13 nm**.

Although the phase that composes the AA and LTE samples is the same, magnetite, the crystals of this phase for the AA sample are approximately 240 nm in size and for the magnetite of the LTE sample they are about 13 nm, a result that was expected since the LTE process achieves much smaller particle sizes, with the consequent reduction of the crystals that form it.

Sample	Phases	Crystalline system	Cell parameters	Crystal size [nm]
AA	Magnetite	cubic (Fd-3m)	a(Å): 8.3750 b(Å): 8.3750 c(Å): 8.3750 Alpha(°): 90.0000 Beta(°): 90.0000 Gamma(°): 90.0000 Z: 8.0000	240 nm
	Goethite	Orthorhombic (Pbnm)	a(Å): 4.6188 b(Å): 9.9528 c(Å): 3.0236 Alpha(°): 90.0000 Beta(°): 90.0000 Gamma(°): 90.0000 Z: 4.0000	90 nm
			a(Å): 4.0494 b(Å): 4.0494	

Al	Aluminium	cubic (Fm-3m)	c (Å): 4.0494 Alpha (°): 90.0000 Beta (°): 90.0000 Gamma (°): 90.0000 Z: 4.0000	115 nm
Fe	Ferrite	cubic (Im-3m)	a (Å): 2.8664 b (Å): 2.8664 c (Å): 2.8664 Alpha (°): 90.0000 Beta (°): 90.0000 Gamma (°): 90.0000 z: 2.0000	240 nm
	Taenite	cubic (Fm-3m)	a (Å): 3.5975 b (Å): 3.5975 c (Å): 3.5975 Alpha (°): 90.0000 Beta (°): 90.0000 Gamma (°): 90.0000 z: 4.0000	45 nm
	Magnetite	cubic (Fd-3m)	a (Å): 8.3750 b (Å): 8.3750 c (Å): 8.3750 Alpha (°): 90.0000 Beta (°): 90.0000 Gamma (°): 90.0000 z: 8.0000	--
LTE	Magnetite	cubic (Fd-3m)	a (Å): 8.3750 b (Å): 8.3750 c (Å): 8.3750 Alpha (°): 90.0000 Beta (°): 90.0000 Gamma (°): 90.0000 Z: 8.0000	13 nm

Table 4. Phases, cell parameters and crystal size of each sample. [24]

Regarding the structural characterisation, RX fluorescence allowed us to know what each nanopowder was composed of. AA was 91.45% Fe, Al was 98.38% aluminium, Fe was 91.61% iron and LTE was 92.34% Fe. In this analysis, other components come out in smaller quantities, such as sulphur from the RX tube. By means of the RX diffraction we can know data of the crystallography of the particles, their size and the compounds that form them. The AA samples consist of ~240 nm magnetite crystals and ~90 nm goethite, Al consists of ~115 nm crystals, Fe consists of 240 nm ferrite and 45 nm taenite and LTE only consists of 13 nm magnetite. The composition of the AA and LTE samples is very similar, they have very similar diffractograms, but LTE has wider peaks due to its smaller crystal size.

5.1.2. Microscope Characterization.

Optical microscope.

The composites ES-X% are observed through the optical microscope in order to perform a visual analysis of the surface of the samples. The samples will be observed using the different magnifications allowed by the microscope in the magnetic materials laboratory, without exceeding the device's resolution limit of a few hundred nanometres. Considering that the particles introduced in the composites are of nanometric order, we do not expect to see them individually, but we will be able to check if there are agglomerations of them formed during the synthesis or curing of the composite.

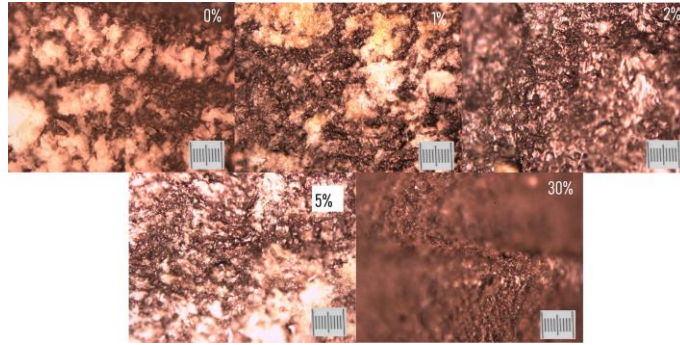


Figure 13. Green magnification of the samples 0, 1, 2, 5 and 30%.

From the images obtained we can conclude that, visually, the agglomerations of the nanoparticles that were introduced as a filler in the composite increase as the concentration of these particles increases, but also, as the concentration of particles in the sample increases, their distribution is more homogeneous, reducing the more punctual agglomerations that may appear with lower percentages of these fillers. For this analysis, we have focused on the yellow and green magnifications, in which the observation of the concentrations is more appreciable.

It should be clarified that the magnifications are clearly visible if the surface of the sample is moderately smooth, due to certain irregularities in the cut of the composites there are certain magnifications that show blurred parts and, in particular, in the sample with a concentration of 9.2% it was impossible to obtain observable images of the green magnification.

SEM microscope.

The distribution of micrometric particles of magnetite in composite matrix has been observed, each sample being doped with different % of Fe₃O₄. For their preparation they have been adhered on double-sided C-tape and metallized with graphite using the Q150T equipment (Quorum Technologies). Images of the three samples have been obtained at 2 or 3 sites of interest in backscattered electron mode (BSE) and some in secondary electron mode (SEI) at magnifications between x100 and x15000, using an accelerating voltage between 20kV. EDX spot analyses have also been performed at some points to check the particle composition [25].

ES-1 Fe₃O₄ 1%:

Some of the images taken of the composite with 1% AA nanoparticles are shown below:

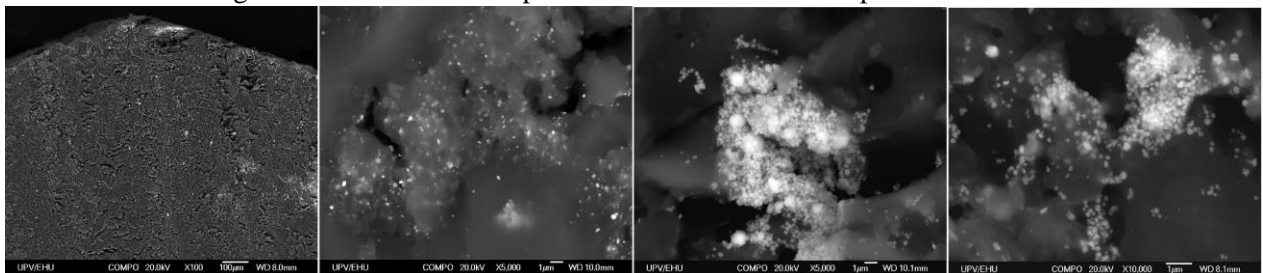


Figure 14. SEM image at different magnifications of ES-1%.

As shown in the figure above, the particle concentration is low and the aggregate formation is also low. There are $3 \cdot 10^{-5}$ aggregates/ μm^2 , with lengths between 2 and 3 μm .

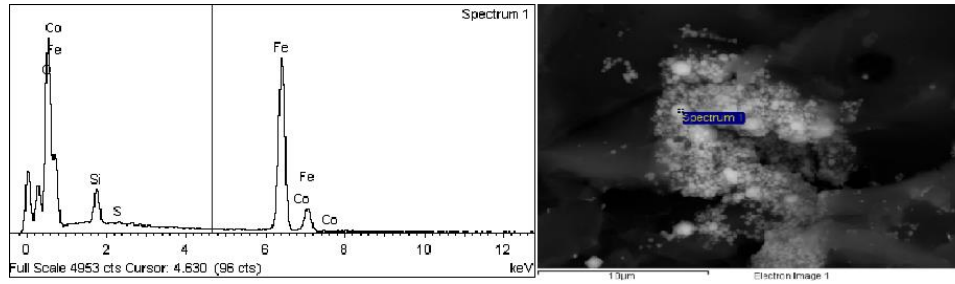


Figure 15. EDX analysis of ES-1%.

EDX analysis of a particle agglomerate shows that the weight percentages of its components are: 54.9% Fe, 40.7% O and about 3% Si. From these data we conclude that the agglomerates, between 2 and 3 microns in size, are formed of iron oxide and that the matrix is silicon based.

ES-5 Fe₃O₄ 5%:

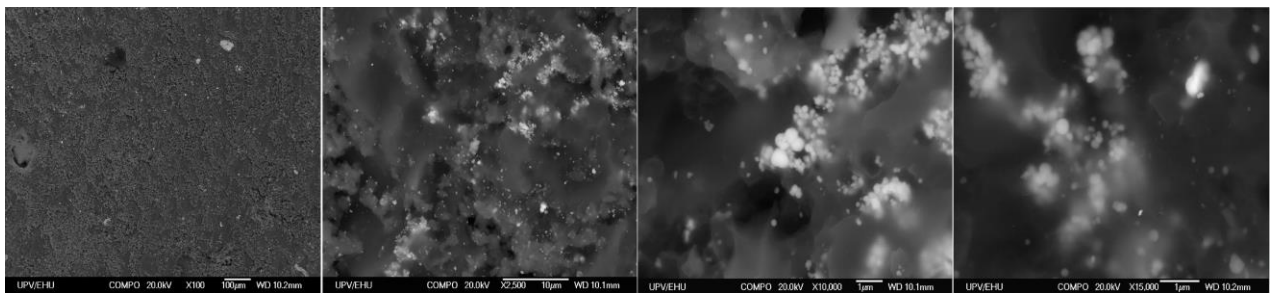


Figure 16. SEM image at different magnifications of ES-5%.

For samples with 5% concentration, there are obviously more particles and more agglomerations of them are formed, around $1.13 \cdot 10^{-4}$ aggregates/ μm^2 , and these agglomerations have larger sizes than the previous ones, between 10 and 70 microns.

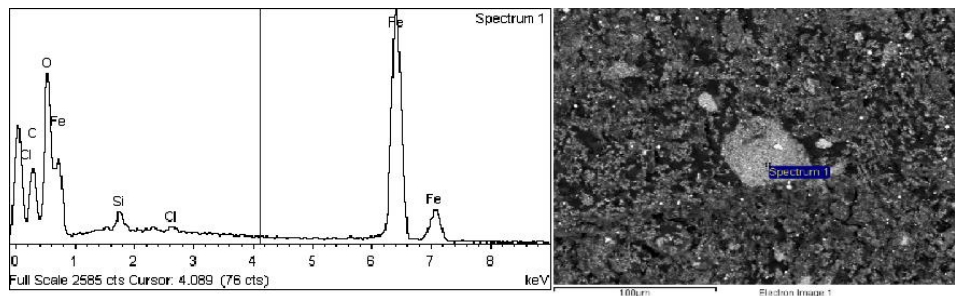


Figure 17. EDX analysis of ES-5%.

EDX analysis of a particle agglomerate shows that the weight percentages of its components are: 65.6% Fe, 31.86% O, 2% Si and 0.6% Cl. From these data we conclude that the agglomerates, are formed of iron oxide and that the matrix is silicon and chlorine.

ES-30 Fe₃O₄ 30%:

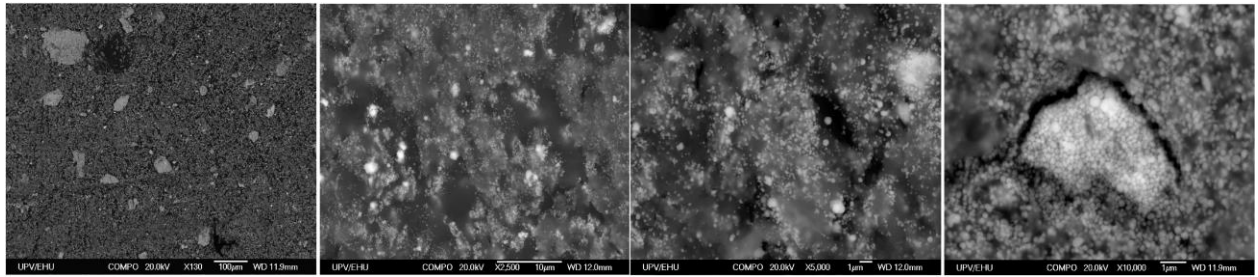


Figure 18. SEM image at different magnifications of ES-30%.

For samples with 30% concentration, the number of particles observed under the microscope is greatly increased and the number of particle agglomerations of about $1.25 \cdot 10^{-3}$ aggregates/ μm^2 , with sizes greater than 100 microns but not exceeding 200 microns, is also increased.

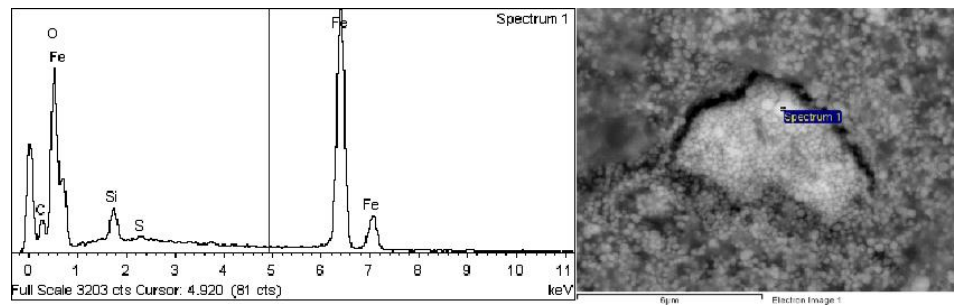


Figure 19. EDX analysis of ES-30%.

EDX analysis of a particle agglomerate shows that the weight percentages of its components are: 63.9% Fe, 32.6% O, 3.2% Si and 0.2% Cl. From these data we conclude that agglomerates larger than 100 microns, between 150 and 170 μm , are formed of iron oxide and that the matrix is silicon and chlorine.

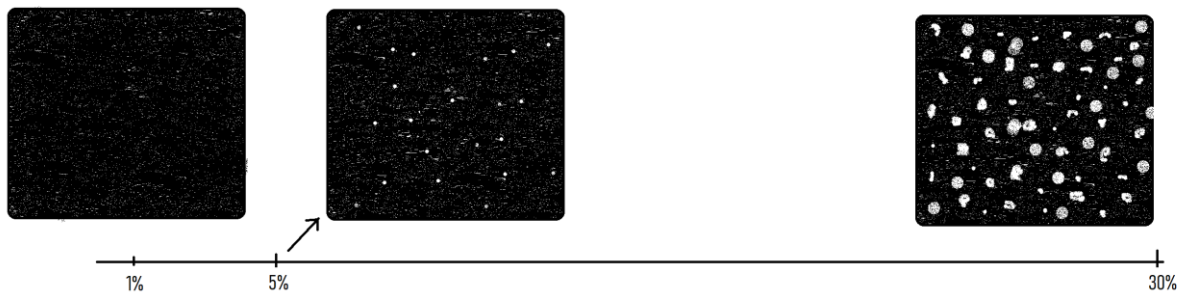


Figure 20. Graphical representation of the aggregates of different concentrations.

The magnetite particles are fundamentally spherical or subspherical and appear dispersed in the matrix individually (variable size, in general $\leq 0.5\mu\text{m}$), forming micrometric aggregates of 2-3 μm in length, or large aggregates of Fe oxides of up to 150-170 μm in the case of sample ES3. Together with magnetite particles it is frequent to find metallic particles with elements of higher atomic number (Cu, Zn, Pb-, Ba-) due to impurities derived from the preparation and/or cutting of the samples.

	Particle's size [nm]	Aggregates' size [μm]	Aggregates' distribution [aggregates/ μm^2]
ES-1	100 nm	2-3 μm	$3 \cdot 10^{-5}$ aggregates/ μm^2
ES-5	100 nm	10-70 μm	$1.13 \cdot 10^{-4}$ aggregates/ μm^2
ES-30	100 nm	100-200 μm	$1.25 \cdot 10^{-3}$ aggregates/ μm^2

Table 5. SEM microphotography information of the samples.

From optical microscopy, analysing the ES-0, 1, 2, 5 and 30% composites, an increase of particles in the composite and with it, an increase of particle agglomerations has been observed, but this is better observed from SEM microscopy. Therefore, from the SEM images of the samples ES-1, 5

and 30%, it can be concluded that the number of agglomerations increases as the concentration of particles increases and that these agglomerations also increase in size, with agglomerations of 2-3 μm for ES-1, between 10 and 70 μm for ES-5 and 150-170 μm for ES-30.

5.2. Analysis of magnetic measurements.

5.2.1. Analysis of powder samples.

Next, the hysteresis cycles of the different nanoparticles in powder form will be shown. For this purpose, the powder will be worked in the VSM 2T with the samples introduced in a capsule with cotton, in order to avoid the movement of the particles and alter the obtaining of the magnetic moment. Through these measurements we know the saturation magnetization of pure nanoparticles, since we analyse a powder that is only composed of nanoparticles. From these measurements we know the saturation magnetization of these materials when they are in nanoparticle form. In addition, we can obtain information on the energy losses in the rearrangement of magnetic domains of the particles through their hysteresis cycles.

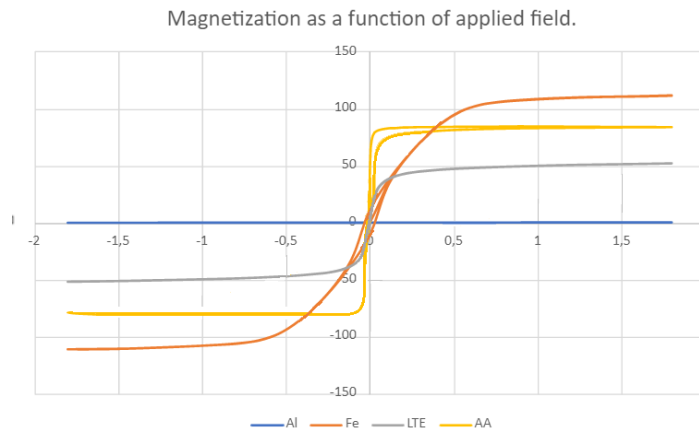


Figure 21. Magnetization as a function of applied field for all the powder samples.

	Ms [emu/g]	Hc [T]	Mr [emu/g]
AA	84.5 emu/g	0.05	9
Al	--	--	--
Fe	111.6 emu/g	0.029	11.1
LTE	51.9 emu/g	0.002	5.6

Table 6. Hysteresis loop information of each sample.

For the powder of commercial magnetite particles, a saturation magnetization of 35.42 emu/g is obtained, with a very small area enclosed by the hysteresis loop, which implies very low energy dissipated as heat [26]. As can be seen, the magnetic behaviour of the aluminium particle powder is practically null, with an extremely low saturation magnetization. There are no energy losses since there is hardly any interaction with the external magnetic field that feeds the VSM. For the powder of the Fe particles, a saturation magnetization of 111.59 is obtained, with low remanence and a slight loss of energy dissipated in the form of heat that is proportional to the area enclosed by the cycle. For the powder of the LTE particles, a saturation magnetization of 51.95 emu/g is obtained, without remanence or loss of energy in the form of heat. It may appear that LTE particles have a superparamagnetic behaviour when looking at their hysteresis curve, but on the other hand, this cannot be confirmed without performing a ZFC-FC analysis.

We can observe that the particles that have a higher saturation magnetization correspond to the Fe and LTE particles that exceed the commercial magnetite particles and of course the Al particles, since the response before the application of a magnetic field of aluminium is practically negligible.

5.2.2. Analysis of ES-X% composites.

A new method for the characterisation of the samples, which will allow us to know if the concentrations of each sample are adequate, is the magnetic analysis of the samples. A vibrating sample magnetometer was used to take these measurements, is a measuring device based on Farady's Law, consisting of the measurement of the armature in a set of coils. voltage induced in a set of coils. This instrument allows the acquisition of different parameters of the samples such as magnetisation, magnetic moment and, therefore, the hysteresis cycle. The operation of this apparatus is based on vibrating a sample at about 60 Hz within a static magnetic field. Once the hysteresis cycles have been obtained, by analysing them, of the different samples manufactured the percentages of these nanoparticles present in each test sample can be determined. In this way we can determine by means of another process the amount of filler present in the composite and corroborate the previous analyses carried out.

These measurements were taken on a vibrating sample magnetron in the faculty of the university. A vibrating sample magnetometer measures the magnetic moment of a sample when it vibrates in the presence of a static magnetic field, which does not exceed 2 Teslas of applied field, from which the magnetisation and magnetic susceptibility can be determined, giving very accurate results. By knowing the magnetic moment of each sample, the concentration of iron particles in each sample can be determined.

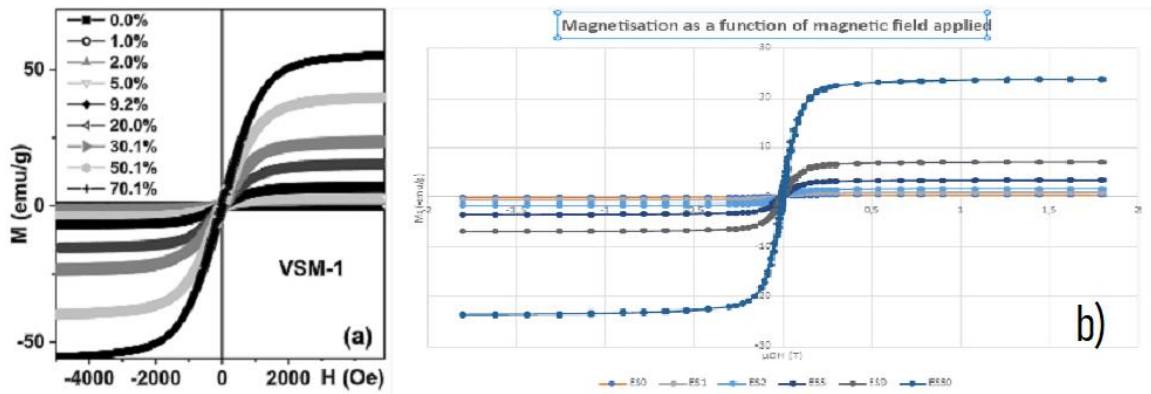


Figure 22. Magnetization as a function of applied field for all the ES-X% composites a) Yekaterinburg b) UPV/EHU.

The following saturation magnetizations are obtained for the different particle concentrations:

Particles concentration	Ms (Yekaterinburg) [emu/g]	Ms (UPV/EHU) [emu/g]
0%	0.000	0.297
1%	0.560	0.789
2%	1.400	1.572
5%	3.200	3.396
9%	6.900	7.011
30%	23.500	23.570

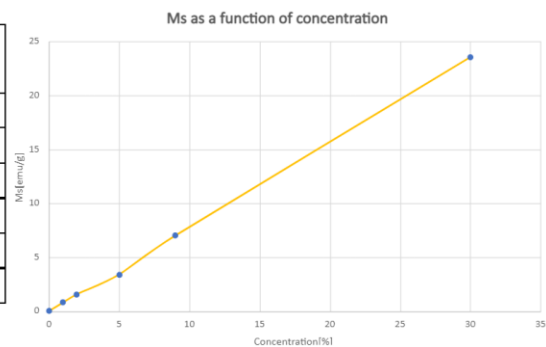


Table 7. Magnetization of the different concentration samples. Figure 23. Ms of the different concentration of AA.

As can be seen in figure x, the saturation magnetisation increases approximately linearly with increasing concentration of AA particles in the composites. The magnetization measurements of these composites were also taken at the state university of Yekaterinburg, Russia, thanks to which it can be verified that the measurements carried out in this work are adequate since the results are similar to those obtained there after carrying out a identical test. In the measurements carried out in Russia, composites with other

concentrations than those were analysed. In addition to the concentrations of 0, 1, 2, 5, 9 and 30%, measurements of the nanoparticle concentrations of 20 and 50% were also taken there.

As can be seen in the tables, the differences between the saturation magnetizations of the different samples are minimal, confirming that the measurements taken at the faculty are correct, under comparison of the results of measurements outside the investigation.

5.2.3. Analysis of composites with 2 and 4 drops of lacquer.

Magnetic characterisation of a series of composites composed of the above-mentioned nanoparticles and a resin is carried out.

The synthesis of these composites is straightforward and two composites are made from each type of particle. The mixture will be approximately 10 mg of nanoparticles together with 2 and 4 drops of the resin. The magnetic characterisation of these composites is the same as those carried out previously, thanks to the VSM 2T instrument, the hysteresis cycles of each one will be obtained.

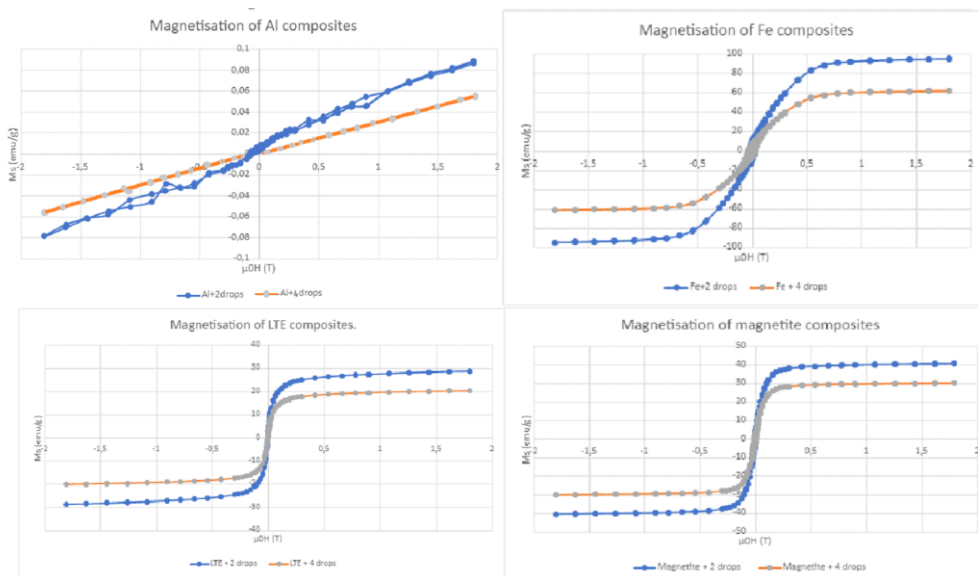


Figure 24. Magnetisation of lacquer composites.

From the mass of the dry composite and the mass of particles in it we can calculate the theoretical percentage of particle concentration in the composite, and comparing the Ms of the nanoparticle powder with the Ms of the composites we can know the practical concentration of particles in the composite, obtaining:

	Powder weight (mg)	Number of drops	Composite's weight (mg)	Dry composite's weight (mg)	Ms [emu/g]	Theoretical %	Practical %
AA	10.81	2	47.3	18.52	40.5	58.4	47.9
AA	10.87	4	85.07	25.80	30.0	42.1	35.5
Al	9.65	2	48.7	16.62	0.9	58.1	--
Al	10.20	4	83.98	24.71	0.6	41.3	--
Fe	10.54	2	45.39	17.77	94.9	59.3	85.0
Fe	10.65	4	85.45	25.30	61.8	42.1	55.4
LTE	10.26	2	44.11	16.88	28.7	60.8	55.3
LTE	10.89	4	83.90	24.49	20.3	44.5	39.1

Table 8. Composition and magnetisation of lacquer composites.

The calculation cannot be performed for Al composites since the M_s of the powder is practically negligible.

About the magnetic measurements, which consist of the analysis of powdered samples or composites. Regarding the VSM measurements of the nanoparticles, we can obtain the magnetic moment of saturation of each of them, in which we obtain, for Fe $M_s = 111.59$ emu/g, $M_s(\text{LTE}) = 51.95$ emu/g, $M_s(\text{AA}) = 35.42$ emu/g and a magnetisation of saturation practically null for the aluminium particles. The same measurements are carried out, but in this case for the ES-0, 1, 2, 5, 9 and 30% composites, the expected saturation magnetisation results are obtained as a function of the AA concentration in each sample. To finalise the magnetic measurements, the samples of lacquer composites with 2 and 4 drops are also analysed in VSM, and the results are again as expected depending on the composition of the composites.

5.3. Microwave absorption.

For the characterization of the microwave absorption properties, two techniques are used, one with a microwave emitter and a microwave receiver and FMR measurements of the different samples. Both absorption and non-absorption of microwave radiation can be an interesting property depending on the intended application of the composites. If the composites are shown to absorb microwave radiation, an important application may be the hyperthermia of cancer cells, whereas if the composites do not absorb microwave radiation, they may have applications where they do not have to interact with microwave radiation, such as for calibrating magnetic sensors. Throughout this section we will learn about the behaviour of samples under microwave radiation.

5.3.1. Transmitter-receiver.

There are many advantages of analysing optical phenomena at microwave frequencies. A transmitter-receiver system will be used, in which the transmitter uses a wave with a wavelength of 2.85 cm and a receiver which can amplify the received signals.

For the development of this method, it is necessary to manufacture a matrix consisting of a plastic rectangle on which 20 capsules are placed adhered with the manufactured composites. Six matrices are synthesized, one that is only the plastic rectangle, another one with capsules containing only lacquer and 4 others with lacquer composites and the 4 types of nanoparticles. For its manufacture, in each capsule is introduced the same mass of nanoparticles ~ 8.20 mg and two drops of lacquer. Once the 20 capsules are synthesized, they are glued to the rectangle forming a matrix of 4 rows and 5 columns.

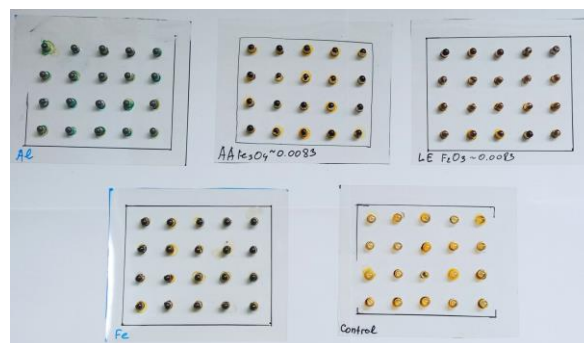


Figure 25. Different composite matrices.

For the development of the measurements the arrays are placed in front of the microwave receiver in order to see if the signal received in the receiver varies. The system comes with a built-in goniometer, with which the angle of incidence can be varied, but in this case, it is not used, only the emitter is moved 1 mm away from the receiver for each measurement.

The receiver voltage is measured as a function of the distance between transmitter and receiver. These are the results obtained:

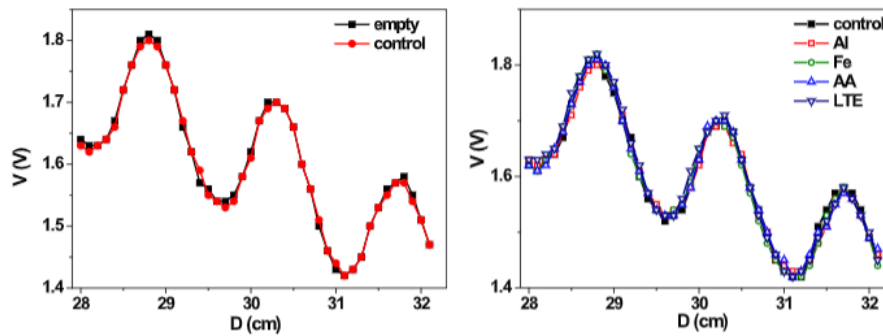


Figure 26. Representation of the absorption diagram of the different matrices.

In the figure 26 we can see 2 different graphs. The one on the left corresponds to the comparison of microwave radiation absorption between the control matrix and no matrix. As can be seen the received voltage signals as a function of distance are identical for the 2 samples.

The graph on the right corresponds to the representation of the absorption of the control, aluminium, AA, LTE and Fe matrices. It can be seen that the microwave radiation behaviour is not affected by the different particle composite matrices, all lines are superimposed. From the technique used it is possible to calculate the wavelength of the wavelength emitted by the emitter, in this way, in the upper graphs the distance between two minima or two maxima corresponds to $\lambda/2$, in this way, averaging all the maxima and minima of the figures we obtain a distance between peaks of 1.45 cm, with an error of ± 1 mm, which gives us a wavelength of $\lambda = 2.90$ cm which does not differ much from the theoretical λ which is 2.85 cm [20].

To compare the effects of radiation, a new matrix is made, with the same proportions as the capsule matrices, but this mixture of lacquer and "AA" particles is spread across the plastic sheet, forming a uniform composite layer. It will be subjected to the same process as the previous laminates and, in addition, the matrix will be subsequently magnetized and absorption measurements will be performed again.

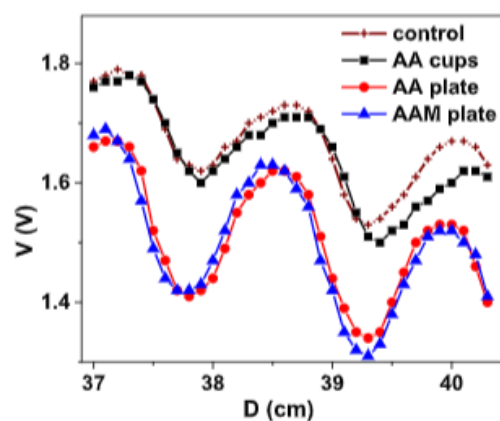


Figure 27. Representation of the absorption diagram of the different matrices.

In the figure above we can see that when the matrix is formed by a uniform composite laminate, there is a decrease in the voltage at the output of the measuring device, although the curve retains the same shape. This decrease of the voltage implies an absorption of the microwave radiation of this matrix. However, there is hardly any difference between the unmagnetized and the magnetized matrix.

As can be seen, from 35 mm onwards, control measurements and AA cups begin to differentiate, this is due to the fact that the measuring instrument is limited, which makes it easy to make measurement errors.

5.3.2. Ferromagnetic resonance (FMR).

Samples were prepared for this test, using approximately 8.3 mg of the nanoparticle powders and 2 drops of lacquer. But not everything is used for the measurements, because depending on the material to be analysed, only a few mg of sample is sufficient to avoid FMR saturation.

The instrument used for FMR calculates the derivative of the microwave radiation absorption as a function of the applied external field. In this way, the following graphs are obtained:

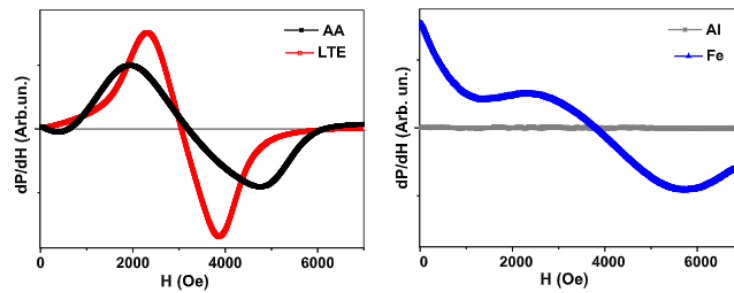


Figure 28. FMR diagrams of the different nano powders.

The figure above has two plots, the one on the left corresponds to the absorption derivatives of the AA and LTE nanoparticles and the one on the right corresponds to the FMR plots of Al and Fe.

	Absorption		Hr [Oe]	ΔHr [Oe]
	resonant	Not resonant		
AA	+	-	3200	2900
Al	-	-	--	--
Fe	-	+	3800	--
LTE	+	-	3050	1700

Table 9. Information of FMR of each sample.

With respect to the graph on the left, it can be seen that the shape of the curve is almost similar, but the distance between the peaks of the LTE particles is smaller and their height is greater, but the absorbance field for both is practically at the same point, above 3000 Oe. What these results indicate is that the behaviour of these two types of particles is similar, but the size of the LTE particles is smaller, which implies these differences in the curves, when ΔHr is larger, it implies a larger particle size. For the graph on the right, we can see that the Al nanoparticles do not absorb the radiation independently of the applied external magnetic field. For the Fe particles we can see that there is absorption for external magnetic fields of 0 Oe, which implies that these particles, although they can absorb electromagnetic radiation, it's not resonant absorption.

From the data obtained, by means of the integration of the derivative of the absorption, the absorption can be calculated. In this way we obtain the absorption of the LTE particles. Furthermore, it can be compared with the absorption measurements, which can also be determined with the FMR instrument:

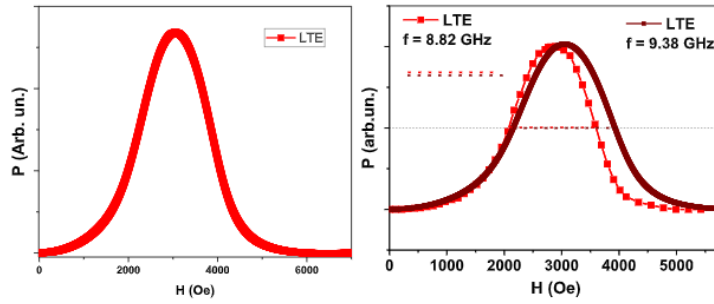


Figure 29. Absorption plots as a function of LTE applied field.

The left graph corresponds to the calculation of the integral of the previously obtained data of the LTE particles, with a resonance field around 3000 Oe. The graph on the right corresponds to the comparison of the curve on the right with an absorption curve measured with the instrument, but at a different frequency. There is a direct dependence between the resonance field and the working frequency of the instrument(3), so that as the frequency increases to 9.38 GHz the resonance field shifts to higher values [22].

$$Hr=2\pi f/8.8 \quad (3)$$

Two types of measurements were carried out to characterise the microwave radiation absorption properties, one for the particles and the other for the composite matrices. The matrices, consisting of 20 capsules of resist and particle composites, were subjected to a radiation emitter-receptor test, whereby it was determined that none of the matrices absorbed microwave radiation. In contrast, another matrix was fabricated with the same quantities as the capsule matrices, but this was a thin homogeneous layer of resist and AA composite, here a considerable increase in radiation absorption was observed for both the unmagnetized and the magnetised matrix. The powder samples were analysed at FMR, from which it was concluded that Al does not absorb radiation, that Fe does not absorb radiation resonantly and that the LTE and AA samples have a very high absorption.

6. Conclusions.

From these characterization techniques applied to the samples we can know the properties of the nanoparticles synthesized from electrophysical techniques.

It can be verified that the laser target evaporation method synthesizes particles much smaller in size and with a good spherical shape compared to the electric wire explosion technique, a quality that can be fundamental for biomedical applications in order to be able to intervene in the least invasive way possible. It has also been found that the composition and structure of the composites, i.e., the occurrence of agglomerations, does not visibly affect the magnetic behaviour of the sample, which is important due to the difficulty of controlling such particle agglomerations. All the particles show a good magnetic behaviour except for the aluminium particles, which is to be expected, allowing them to be used for various technological applications, such as nano sensors or sensor calibrators, or biomedical applications such as hyperthermia or thermoablation.

Regarding their behaviour in absorption of microwave radiation, the arrays synthesized with 20 capsules glued on a plastic sheet did not absorb absolutely none of the radiation to which they were exposed, which may be interesting for various devices that work under this radiation, but should not be altered by it. On the other hand, when the matrix was synthesized with a thin layer of composite, it did increase its microwave absorption, which makes it a suitable material for radar or wireless antenna systems. As for the resonant absorption measurements, only the AA and LTE particles performed adequately, making them suitable for magnetic positioning sensor applications.

A great boom is expected in the knowledge of the behaviour of nanoparticles synthesized by electrophysical techniques, which achieve spherical shapes, smaller sizes and less contamination, since they represent a very important advance in current technology and are becoming increasingly important in the field of biomedicine.

7. References.

- [1] Il'inova, K. O., Safronov, A. P., & Beketov, I. V. (2021). Influence of the Chemical Composition of an Epoxy Resin and of Its Filling with Nanoparticles of Iron, Aluminum, and Their Oxides on the Enthalpy of Curing with m-Phenylenediamine. *Russian Journal of Applied Chemistry*, 94(8), 1072-1079.
- [2] Zhang, X., Hao, H., Shi, Y., & Cui, J. (2015). The mechanical properties of Polyvinyl Butyral (PVB) at high strain rates. *Construction and building materials*, 93, 404-415.
- [3] Kumar, P., Khan, N., & Kumar, D. (2016). Polyvinyl butyral (PVB), versatile template for designing nanocomposite/composite materials: a review. *Green Chem. Technol. Lett*, 2(4), 185-194.
- [4] Kurlyandskaya, G. V., Safronov, A. P., Shcherbinin, S. V. E., Beketov, I. V., Blyakhman, F. A., Makarova, E. B., ... & Svalov, A. V. (2021). Magnetic nanoparticles obtained by electrophysical technique: focus on biomedical applications. *Physics of the Solid State*, 63(10), 1447-1461.
- [5] Hyeon, T. (2003). Chemical synthesis of magnetic nanoparticles. *Chemical communications*, (8), 927-934.
- [6] Gericke, M., & Pinches, A. (2006). Biological synthesis of metal nanoparticles. *Hydrometallurgy*, 83(1-4), 132-140.
- [7] Kurlyandskaya, G. V., Bhagat, S. M., Safronov, A. P., Beketov, I. V., & Larrañaga, A. (2011). Spherical magnetic nanoparticles fabricated by electric explosion of wire. *AIP Advances*, 1(4), 042122.
- [8] Safronov, A. P., Beketov, I. V., Komogortsev, S. V., Kurlyandskaya, G. V., Medvedev, A. I., Leiman, D. V., ... & Bhagat, S. M. (2013). Spherical magnetic nanoparticles fabricated by laser target evaporation. *AIP Advances*, 3(5), 052135.
- [9] Kurlyandskaya, G. V., Safronov, A. P., Bhagat, S. M., Lofland, S. E., Beketov, I. V., & Prieto, L. M. (2015). Tailoring functional properties of Ni nanoparticles-acrylic copolymer composites with different concentrations of magnetic filler. *Journal of Applied Physics*, 117(12), 123917.
- [10] Kurlyandskaya, G. V., Safronov, A. P., Terzian, T. V., Volodina, N. S., Beketov, I. V., Lezama, L., & Prieto, L. M. (2015). Fe 45 Ni 55 magnetic nanoparticles obtained by electric explosion of wire for the development of functional composites. *IEEE Magnetics Letters*, 6, 1-4.
- [11] Blyakhman, F. A., Buznikov, N. A., Sklyar, T. F., Safronov, A. P., Golubeva, E. V., Svalov, A. V., ... & Kurlyandskaya, G. V. (2018). Mechanical, electrical and magnetic properties of ferrogels with embedded iron oxide nanoparticles obtained by laser target evaporation: Focus on multifunctional biosensor applications. *Sensors*, 18(3), 872.
- [12] Beckhoff, B., Kanngießer, B., Langhoff, N., Wedell, R., & Wolff, H. (Eds.). (2007). *Handbook of practical X-ray fluorescence analysis*. Springer Science & Business Media.
- [13] Warren, B. E. (1941). X-ray diffraction methods. *Journal of applied physics*, 12(5), 375-384.
- [14] Bunaciu, A. A., Udriștioiu, E. G., & Aboul-Enein, H. Y. (2015). X-ray diffraction: instrumentation and applications. *Critical reviews in analytical chemistry*, 45(4), 289-299.
- [15] Davidson, M. W., & Abramowitz, M. (2002). Optical microscopy. *Encyclopedia of imaging science and technology*, 2(1106-1141), 120.
- [16] Mohammed, A., & Abdullah, A. (2018, November). Scanning electron microscopy (SEM): A review. In *Proceedings of the 2018 International Conference on Hydraulics and Pneumatics—HERVEX, Băile Govora, Romania* (pp. 7-9).
- [17] Foner, S. (1996). The vibrating sample magnetometer: Experiences of a volunteer. *Journal of applied physics*, 79(8), 4740-4745.
- [18] Lubell, M. S., & Venturino, A. S. (1960). Vibrating sample magnetometer. *Review of Scientific Instruments*, 31(2), 207-208.

- [19] Aguilar, C. M., Svalov, A. V., Kharlamova, A. A., Shalygina, E. E., Larrañaga, A., Orue, I., & Kurlyandskaya, G. V. (2021). Magnetic and Microwave Properties of FeNi Thin Films of Different Thicknesses Deposited Onto Cyclo Olefin Copolymer Flexible Substrates. *IEEE Transactions on Magnetics*, 58(2), 1-5.
- [20] Scientific, P. (1998). Instruction Manual and Experiment Guide for the PASCO Microwave Optics Set Model WA: 9314B. Canada: Pasco.
- [21] Spano, M. L., & Bhagat, S. M. (1981). Ferromagnetic resonance in amorphous alloys. *Journal of Magnetism and Magnetic Materials*, 24(2), 143-156.
- [22] Kurlyandskaya, G. V., Cunanan, J., Bhagat, S. M., Apesteguy, J. C., & Jacobo, S. E. (2007). Field-induced microwave absorption in Fe₃O₄ nanoparticles and Fe₃O₄/polyaniline composites synthesized by different methods. *Journal of Physics and Chemistry of Solids*, 68(8), 1527-1532.
- [23] Patterson, A. L. (1939). The Scherrer formula for X-ray particle size determination. *Physical review*, 56(10), 978.
- [24] Amigó, J. M. (2002). La difracción de rayos X de materiales policristalinos desde la época del Profesor Amorós hasta la actualidad. *Boletín de la Real Sociedad Española de Historia Natural (Sección Geológica)*, 97, 97-112.
- [25] Scimeca, M., Bischetti, S., Lamsira, H. K., Bonfiglio, R., & Bonanno, E. (2018). Energy Dispersive X-ray (EDX) microanalysis: A powerful tool in biomedical research and diagnosis. *European journal of histochemistry: EJH*, 62(1).
- [26] Márquez, M. A. V. EL CICLO DE HISTÉRESIS EN MATERIALES FERROMAGNÉTICOS.